NIH Public Access
Author Manuscript
J Immunol. Author manuscript; available in PMC 2013 November 15.

Published in final edited form as:
J Immunol. 2012 November 15; 189(10): 4870–4880. doi:10.4049/jimmunol.1201296.

NK Cell Lytic Granules are Highly Motile at the Immunological Synapse and Require F-Actin for Post-degranulation Persistence[1]

Emily M. Mace[†,2], **Winona W. Wu**[‡,2], **Tina Ho**[*], **Shaina S. Mann**[‡], **Hsiang-Ting Hsu**[‡‡], and **Jordan S. Orange**[†,§]

[†]Baylor College of Medicine, Houston, Texas, United States of America

[*]University of Pennsylvania School of Medicine, Philadelphia, Pennsylvania, United States of America

[‡]University of Pennsylvania College of Arts and Science, Philadelphia, Pennsylvania, United States of America

[‡‡]Department of Pathology and Immunology, Baylor College of Medicine, Houston, Texas, USA

[§]Texas Children's Hospital, Houston, Texas, United States of America

Abstract

The formation of a dynamic, actin-rich immunological synapse (IS)[3] and the polarization of cytolytic granules towards target cells are essential to the cytotoxic function of NK cells. Following polarization, lytic granules navigate through the pervasive actin network at the IS in order to degranulate and secrete their toxic contents onto target cells. We examined lytic granule motility and persistence at the cell cortex of activated human NK cells using high resolution total internal reflection microscopy (TIRFm) and highly quantitative analysis techniques. We illustrate that lytic granules are dynamic and observe substantial motility at the plane of the cell cortex prior to, but not after degranulation. We also show that there is no significant change in granule motility in the presence of Latrunculin A (which induces actin depolymerization), when added after granule polarization, but that there is a significant decrease in lytic granule persistence subsequent to degranulation. Thus, we show that lytic granules are highly dynamic at the cytolytic human NK cell IS prior to degranulation and that the persistence of granules at the cortex following exocytosis requires the integrity of the synaptic actin network.

INTRODUCTION

NK cells are the cytotoxic effectors of the innate immune system and detect virally infected, tumorigenic or otherwise stressed cells using germline encoded activating receptors. Upon encountering a susceptible target, NK cells can mediate directed cytotoxicity following the formation of an IS and exocytosis of specialized secretory lysosomes, which contain the lytic effector molecules perforin and granzyme (reviewed in (1)). The steps leading to NK cell granule exocytosis are highly regulated, as human NK cells are pre-armed with

[1]Supported by NIH-NAIAD R01067946

[3]Abbreviations used in this study: IS, immunological synapse; TIRFm, total internal reflection microscopy; LatA, Latrunculin A; AU, arbitrary units; MTOC, microtubule organizing center.

Corresponding Author: Jordan S. Orange, Phone: (832) 824-1319, Fax: (832) 825-1260, orange@bcm.edu.
[2]These authors contributed equally to this work.

NIH-PA Author Manuscript
NIH-PA Author Manuscript
NIH-PA Author Manuscript

NIH-PA Author Manuscript

NIH-PA Author Manuscript

NIH-PA Author Manuscript

constitutively mature lytic granules and need not undergo further activation or expansion in order to kill (2, 3).

NK cell lytic granule exocytosis is preceded by the dynein-dependent convergence of granules to the microtubule organizing center (MTOC) and subsequent polarization of the MTOC and granules to the IS (4). Once polarized, lytic granules undergo docking and fusion with the NK cell membrane, after which their contents can be released upon the target cell. A dynamic actin cytoskeleton is required for multiple aspects of cytotoxicity and IS maturation, including lytic granule polarization and degranulation (5, 6). Furthermore, the association of granules with actin filaments in a pervasive actin network suggests a role for actin specifically in granule trafficking immediately prior to exocytosis (5, 7, 8). The actin motor protein myosin IIA, which is also required for degranulation, is found both at the IS and the surface of lytic granules, and inhibition or loss of myosin IIA function results in impaired delivery and movement of granules at the plasma membrane (9, 10).

In order to address the question of lytic granule delivery and the role of the cytoskeleton in this process, we sought to determine the behavior of granules at the plasma membrane of activated human NK cells. We employed total internal reflection fluorescence microscopy (TIRFm) since it is designed for accurate visualization of objects within 150nm of a glass surface. Thus, we used TIRFm to study only those granules present at the NK cell plasma membrane in living cells by utilizing vital labeling with LysoTracker Red and a constitutively expressed lysosomal activation marker protein 1 (LAMP1)- fluorescent reporter. We have previously designed the LAMP1-pHlourin reporter to identify degranulation events in living cells, since the construct allows for the sorting of LAMP1-pHluorin to lytic granules, with the pHluorin contained within the granule (5). At baseline lytic granule acidic pH the pHlourin does not fluoresce, but when the granule pH changes to a more neutral pH upon degranulation the phluorin can be excited to fluoresce green. Use of these technologies allowed us to identify and track individual granules both before and after exocytosis. We found that individual granules underwent dynamic, undirected movement at the plasma membrane prior to, but not following, fusion and release of granule contents. Surprisingly, depolymerization of the actin cytoskeleton with Latrunculin A (LatA) did not affect pre-exocytosis lytic granule movement. The integrity of the actin cytoskeleton, however, was required for persistence of granules following fusion, defining a specific interplay between NK cell lytic granules and synaptic actin as well as a role for synaptic actin in degranulation.

MATERIALS AND METHODS

Cell lines

The NK92 pHlourin-LAMP1 cell line (5) and YTS GFP-actin (11) cell lines were generated previously. All NK cell and 721.221 and K562 target cell lines were maintained as described (12).

Live cell confocal microscopy

For imaging of NK cells with target cells, NK cells (effectors) were suspended in RPMI 10% FBS at a concentration of 10^6 cells/ml and incubated with 10 μM LysoTracker Red DND-99 at 37° for 30 minutes then washed and suspended in media. Effectors were mixed at a 2:1 ratio with target cells that had been pre-incubated for 5 minutes with 5 μg/ml CellMask Plasma Membrane Stain (Invitrogen). Conjugates were plated in Lab-Tek #1.0 borosilicate chamber slides (VWR) that had been coated with 5μg/ml anti-CD48 (BD clone TU145) for 30 minutes at 37° then washed 3 times to adhere target cells and thus facilitate imaging. Effectors and target cells were incubated for 30 minutes then SYTOX Blue was

NIH-PA Author Manuscript

NIH-PA Author Manuscript

NIH-PA Author Manuscript

added to a final concentration of 1 μM. For NK92 LAMP1-pHluorin experiments, conjugates were imaged on a Leica SP8 laser scanning confocal microscope with 100× 1.45 NA objective. Excitation was provided by a UV laser at 405 nm and tunable white light laser at 488-, 561 and 647 nm. Emission was detected with HyD detectors and images were collected in a single *z*-plane at one frame per minute for 60–150 minutes. Data was acquired with LAS AF software (Leica) then exported to Volocity (Perkin Elmer) for analysis. For NK92 and YTS conjugates, cells were imaged in a single plane on a Zeiss Axioplan Observer Z1 fluorescence microscope with a 63× 1.40 NA objective and Yokigawa CSU-10 spinning disk with excitation by 405-, 488-, and 568- and 647- nm lasers in LMM5 laser combiner unit (Spectral Applied Research). Images were acquired for 90–130 minutes at a rate of one frame per minute using Volocity software (PerkinElmer). Temperature was maintained at 37° using a ΔT dish heater and lid (Bioptechs).

Live cell TIRFm

For NK92 lytic granule motility studies, pHluorin-LAMP1 NK92 cells were suspended in dye free RPMI 10% FBS media at a concentration of 7.5×10^5 to 10^6 cells/ml and incubated with 100 nM Lysotracker Red DND-99 (Invitrogen) at 37°C for 30 minutes, washed, and resuspended in media. ΔT culture dishes (Bioptechs) were coated with 5μg/ml anti-NKp30 and -CD18, incubated at 37°C for 1 hour or 4 degrees overnight, washed with PBS, and pre-warmed with dye free RPMI 10% FBS media. NK92 cells were plated on ΔT culture dishes immediately prior to imaging, and temperature was maintained at 37°C throughout the experiment using a ΔT culture dish heater and lid (Bioptechs).

Cells were imaged in a single *z*-axis plane 10–15 minutes after addition to imaging chambers through an APO N TIRFm, oil immersion 60× 1.49 NA objective using an Olympus IX-81 spinning disk confocal microscope with a rear-mounted TIRF illuminator and a Hamamatsu EM CCD C9100 camera. Excitation was provided by 480 nm (Spectra-Physics) and 561 nm (Cobalt) diode lasers through a LMM5 laser combiner unit (Spectral Applied Research). Cell image sequences were captured in TIRF mode at the interface between the cell and the glass over 60–80 minutes at 6 frames per minute using Volocity software (PerkinElmer). Where indicated, 10 μM LatA (Sigma) or DMSO (Fisher Scientific) was added to cells in the imaging chamber, but only after 10 minutes of incubation had elapsed.

Image Analysis

For analysis of live NK cell conjugates, images were identified and cropped in Volocity (PerkinElmer). The centroid of the entire combined lytic granule region was identified at each time point using Volocity software (PerkinElmer) centroid to IS distance was measured via the shortest line connecting this point to the IS as described previously (4). The mean centroid to IS distance was calculated across independently repeated cell observations as a feature of the timepoint after activation. Mean fluorescent intensity of SYTOX Blue staining was measured for each time point in Volocity and exported to GraphPad Prism version 5.0 (GraphPad software).

For TIRFm analysis, image sequences were analyzed using Volocity software (PerkinElmer). LysoTracker Red and pHluorin positive events were identified and cropped in Volocity. Object tracks were generated over time using the “track objects manually” function and the rectangular selection tool for each event; the track length, track velocity, displacement, and displacement rate of each lytic granule were measured for both LysoTracker Red time points and pHluorin time points, and comparatively graphed on GraphPad Prism Version 5.0 (GraphPad software). Plotting X and Y coordinate values from Volocity with GraphPad Prism generated overlays of lytic granule tracks for both

NIH-PA Author Manuscript

NIH-PA Author Manuscript

NIH-PA Author Manuscript

Lysotracker Red and pHluorin. To measure the time of visibility of LysoTracker Red lytic granules within the TIRF field, the time of LysoTracker Red emergence on the TIRF field was subtracted from the time of pHlourin appearance or LysoTracker Red disappearance and multiplied by 60 to obtain time in seconds.

For LatA experiments, granules with both Lysotracker Red and pHluorin traces were identified and cropped in Volocity. Objects were identified using a threshold of 3 SD above the mean field fluorescence for each timepoint to account for photobleaching using the "Find Objects Using SD Intensity" function. Objects smaller than 0.032 μm^2 were excluded from further analysis. Tracks were then generated using the "Track Objects" feature using the "Shortest Path" tracking model, and the track length, track velocity, displacement, displacement rate, and time span of each lytic granule graphed using GraphPad Prism software Version 5.0.

The sum fluorescent intensity and area of each granule was also recorded at each time point. Using the initial appearance of pHluorin-LAMP1 as time zero, the average sum fluorescent intensity post-degranulation was calculated and graphed for lytic granules treated with DMSO vehicle control versus those treated with LatA. For area measurements, the borders of individual granules were defined as those above 3 SD.

Statistical Analysis

The minimum sample size of lytic granules required for evaluation in a given experiment was determined using a DSS sample size calculator, with α and β error levels of 1% (DSS Research). Statistical significance was determined by performing two sample, unpaired, two-tailed *t* tests or Mann Whitney U tests using GraphPad Prism version 5.0 (GraphPad Software). Differences were considered to be significant if $p < 0.05$. All error bars shown represent SD.

RESULTS

Polarization of lytic granules to the IS precedes their synaptic persistence prior to target cell death

We sought to analyze the dynamics of NK cell lytic granule convergence, polarization and target cell death in live NK cells. YTS GFP-actin cells were loaded with LysoTracker Red DND-99, which selectively labels acidified organelles and fluoresces at 568 nm in acidic pH. Susceptible 721.221 target cells were labeled with CellMask in order to discern them from effector cells and NK-target cell conjugates were imaged every sixty seconds for 60–120 minutes via live cell spinning disk confocal microscopy. Imaging was performed in the presence of SYTOX Blue nucleic acid stain, which does not permeate the membrane of living cells and thus identifies dying cells within the population. Following initial contact with target cells, NK cell granules were observed to rapidly converge to the MTOC as has been previously reported (4). This was then followed by polarization of granules to the IS (Figure 1A, top panel, Supplementary Video 1). While granule polarization occurred rapidly, the initiation of target cell death as marked by SYTOX entry was not visualized until approximately one half-hour later (Figure 1A, bottom panel, Supplementary Video 1). Analysis of ten conjugates supported this observation, with the mean time of granule polarization measured as 41.5 ± 12 minutes (Figure 1B) and SYTOX Blue entry being first observed at a mean time of 61.5 ± 14 minutes (Figure 1C). During this time granules remained converged at the MTOC and continued to be visible, suggesting they were not undergoing degranulation or recycling. Thus, granule polarization preceded initiation of target cell death by approximately 20 minutes.

NIH-PA Author Manuscript

NIH-PA Author Manuscript

NIH-PA Author Manuscript

To ensure that these observations were not specific to the YTS cell line, these same parameters were studied in a second and distinct NK cell line. We imaged NK92 GFP-tubulin NK cells conjugated to susceptible K562 targets using the same strategy as above. Similar to YTS-mediated target cell apoptosis, NK92 mediated target cell death was delayed following granule polarization. Quantitation of 6 cell conjugates confirmed this observation, with a mean time of granule polarization of 24.2 minutes (Figure 1D), and a mean time of initiation of target cell death of 54.2 minutes (Figure 1E). Thus, in a distinct NK cell line, the elapsed time between granule polarization and onset of target cell death was also delayed and with these NK cells was approximately 30 minutes.

Finally, to visualize the polarization of granules relative to target cell death with reference to NK cell degranulation on a single cell level, we used NK92 cells expressing a pH sensitive GFP mutant fluorescent protein (pHlourin) fused to LAMP1 to visualize individual degranulation events. LAMP1 (CD107a) is sorted to lytic granules and is often used as a marker of degranulation when found on the cell surface (13, 14). At acidic pH within lytic granules pHlourin-LAMP1 is not excited by green wavelengths, but following degranulation and exposure to neutral pH, the pHluorin exhibits fluorescence characteristics of GFP and green emission is observed (5, 15). To identify granules prior to degranulation, NK92 LAMP1-pHlourin cells were loaded with LysoTracker Red. Therefore, individual granules could be tracked over time and degranulation events observed by a transition from red fluorescence, derived from LysoTracker red in acidified organelles, to green fluorescence derived from the neutralization of pH and subsequent activation of LAMP1-pHlourin.

Using this strategy to visualize both granules and degranulation events NK92 LAMP1-pHlourin NK cells were conjugated with K562 targets and imaged live using spinning disc confocal microscopy. As seen in Figure 2 and Supplementary Video 2, granule polarization was marked by movement of red LysoTracker loaded granules to the cell membrane. This occurred relatively rapidly in the example shown, with maximum polarization by 16 minutes following ten minutes of contact (Figure 2B). The progress of granules towards the IS was followed by NK cell degranulation, as marked by a transition from green to red granule fluorescence at the plasma membrane. Initial, transient degranulation events were seen as early as 6 minutes following granule polarization (Figure 2B). These early degranulation events, however, did not persist with each lasting less than five minutes. The early transient degranulations were followed by later events beginning at 25 minutes that were sustained until the end of imaging. Target cell death, as evidenced by a surrogate measure, membrane blebbing, began at approximately 40 minutes (2). Analysis of 4 time-lapse conjugates showed relatively consistent times of polarization, as seen in Figure 1, but highly variable times of initial degranulation events demonstrated by the appearance of LAMP1-pHlourin at the membrane (Figure 2C).

Lytic granules are dynamic prior to, but not following, degranulation at the NKIS

In order to better understand the nature of the polarized lytic granule, its transition to degranulation, and behavior thereafter, we recapitulated the NK cell immune synapse using activating antibodies immobilized on a glass surface, thus allowing for orientation of the NK cell synapse in the XY plane to enable high resolution imaging. We used antibody to the natural cytotoxicity receptor NKp30 and CD18, the β2 subunit of LFA-1, to activate NK cells for degranulation. Together, these signals induce polarized secretion of lytic granule contents and degranulation in the XY plane (5, 16). This approach also allows for visualization of degranulation events by TIRFm, which provides high resolution imaging limited to the membrane proximal 100 nm of cells bound to antibody-coated glass. As above, we used NK92 LAMP1 pHluorin NK cells labeled with Lysotracker Red in order to analyze individual prior to, during and after degranulation at the NK cell plasma membrane.

NIH-PA Author Manuscript

NIH-PA Author Manuscript

NIH-PA Author Manuscript

Cells were imaged using two-color TIRFm at the interface between the cell and the glass in the *XY* plane over time in heated imaging chambers following ten minutes of contact. Numerous polarized lytic granules, indicated by red fluorescence derived from LysoTracker Red labeling, were identified at the plane of the IS. In contrast, degranulation events (red to green color transition) were visualized less frequently at the plane of the cell cortex and observed within the TIRF field over time (Figure 3A, Supplementary Video 3).

To quantify granule behavior after polarization to the IS, individual LysoTracker Red labeled lytic granules undergoing degranulation were measured and tracked in the *XY* plane using TIRFm. Prior to degranulation, an overlay of these tracks at the synapse showed seemingly random, yet highly dynamic, movement of granules navigating the cell cortex (Figure 3B). Tracks of the same granules following degranulation, however, demonstrated greatly reduced motility, as seen by shorter tracks with less displacement (Figure 3C). This observation was further quantitated by measurement of track length, velocity, displacement and displacement rate. Strikingly, pre-degranulation granules had longer track lengths, with a mean length of 10.2±4.2μm compared to 1.0±0.7 μm following degranulation (Fig 4A). The mean velocity for granules pre-degranulation was 0.005μm/sec±0.002, whereas any post-degranulation granule velocity was almost tenfold less, 0.0005±0.0003 μm/sec (Figure 4B). In addition to track length, granules prior to degranulation had a greater displacement from their point of origin, 1.2±0.6 μm when compared to post-degranulation, 0.2±0.1 μm (Figure 4C). Finally, the rate of this displacement in granules prior to degranulation, 0.0005±0.0005μm/sec, was greater than that following degranulation, 0.0001±0.00007μm/sec (Figure 4D). Thus, lytic granules are dynamic and demonstrate considerable non-directed motility at the NK cell IS while navigating the cell cortex before degranulation. Following degranulation, this motility is significantly reduced.

Degranulation events do not predict pre-degranulation motility and persistence

It has been observed that many more NK92 lytic granules approximate the IS than degranulate (5). As a result, a significant number of polarized granules that navigate the IS are not exocytosed. Since it was unclear if the dynamics of these granules would be the same as those that degranulated, we investigated the dynamics of synaptic lytic granules that do not degranulate. Individual Lysotracker Red labeled lytic granules that did not result in degranulation events were distinguished by a consistent, unchanging red fluorescence. These were measured and tracked in the XY plane throughout the duration of imaging until they disappeared from the TIRF field (Figure 5A, Supplementary Video 4). Relative to LysoTracker Red labeled NK92 granules that degranulate, those that do not degranulate were similarly dynamic. An overlay of lytic granule approximation tracks showed considerable non-directed movement (Figure 5B). These lytic granules had lateral mobility that was not significantly different from those that go on to degranulate. The track velocity of granules that did not degranulate was 0.004±0.001 μm/sec, which was not significantly different from the mean of those that degranulate (Figure 6A). Similarly the mean track length of 11.5±3.3 μm, for granules which did not degranulate, was comparable to the track length of those that degranulated (Figure 6B). The mean displacement and displacement rate of granules that did not degranulate was 1.3±0.9 μm and 0.0004±0.0003 μm/sec respectively, which was also not significantly different from the displacement and displacement rate for those that degranulated (Figure 6C, D). Thus, irrespective of whether approximation leads to degranulation, lytic granules have characteristic dynamics at the NK activating IS.

There was, however, considerable variability in the duration of granule persistence within the synapse. To determine if degranulation impacted the persistence of Lysotracker Red labeled lytic granule tracks, the previously identified approximation events were compared. The difference between the time of visibility of LysoTracker Red signal of lytic granules

NIH-PA Author Manuscript

NIH-PA Author Manuscript

NIH-PA Author Manuscript

that did not degranulate, 45.8±12.1 minutes, and those that did, 39.0±14.2 minutes, was not significantly different (Figure 6E). The length of visibility of signal at the synapse also did not affect granule dynamics. A subset of granules were visible for >55 minutes and until the end of imaging (and thus did not degranulate or withdraw). These prolonged non-degranulated events were identified and analyzed throughout their lifetime. Despite their prolonged presence at the synapse, these granules had similar kinetics to both those that degranulated and those that withdrew earlier (Supplemental Figure 2).

Degranulation is accompanied by a significant decrease in the velocity of lytic granules prior to the degranulation event (Figure 4). To determine if all granules undergo similar changes in velocity, we plotted the velocity of granules against time. As shown in Figure 6F, all granules have a reduction in velocity over time. This suggests that the mechanism of arrest of granules at the synapse is independent of that of degranulation. In addition, lytic granules at the cell cortex that do not degranulate have time of persistence and lateral mobility at the cortex that is statistically indistinguishable from that of those that do. Thus synaptic granule arrest precedes, but does not mandate degranulation.

Cortical actin integrity is required for post-degranulation persistence but not pre-degranulation motility

Actin cytoskeleton integrity and remodeling is required for NK cell cytotoxicity. Treatment with the actin polymerization inhibitor LatA rapidly depolymerizes NK cell cortical actin filaments (5) and abrogates cytotoxic function (6, 17). We used LatA to investigate the role of actin in supporting synaptic granule motility at the cortex. Specifically, NK92 LAMP1-phlourin cells were treated with 10 μM LatA or vehicle control (DMSO) 10 minutes after being added and the lytic granules were observed via TIRFm. Surprisingly, pre-degranulation motility of individual granules in LatA-treated cells was intact and similar to those in control-treated cells (Figure 7A, B, Supplementary Videos 5 & 6). Despite LatA-treatment, granules continued to demonstrate motility prior to, but not after degranulation (as measured by a shift from red to green fluorescence) (Figure 7A, B, final panel). Measurement of 12–18 tracks from LatA treated and control treated cells, normalized to the values to the DMSO control, demonstrated no significant differences in lytic granule track length, velocity and total displacement attributable to LatA (Figure 7C).

The major difference following LatA treatment, however, was that of granule lifetime. Granules for which termination of degranulation was observed (as marked by the disappearance of green fluorescence) were selected and timespan measured of the granule both pre- and post-degranulation. There was no difference in the measured lifetime of red fluorescence of granules in Latrunculin A treated cells, 1.1±0.6 AU compared to normalized control treated cells (1.0±0.9). This suggested that the time to degranulation was not affected by LatA. However, when compared to DMSO treated control cells, degranulated granules in LatA treated cells persisted for significantly less time, as measured by a shorter timespan of green fluorescence, 0.6±0.4 AU compared to control 1.0±0.6 (normalized) (Figure 7D, $p=0.04$). This suggests that actin integrity is required for the maintenance of degranulation events at the plasma membrane.

Loss of actin integrity leads to increased granule area

While some granules' green fluorescence was visible through the complete imaging time course (60–80 minutes), other granules ceased to be visible in TIRF field following degranulation. This suggested that the "disappearing" degranulation events were withdrawn into the cell and therefore out of the field of TIRF. Alternatively, the lumenal LAMP1-pHlourin of degranulated events was diluted by diffusion throughout the membrane adjacent to the site of degranulation and was thus falling below the threshold for detection by

NIH-PA Author Manuscript

NIH-PA Author Manuscript

NIH-PA Author Manuscript

imaging. To begin to distinguish between these possibilities, the persistence of granules was plotted using a Kaplan-Meier survival curve (Figure 8A). As imaging continued for variable times following degranulation, some imaging sequences ended with granules still visible (vertical ticks, Fig 8A). However, compared to granules from DMSO treated cells, those from LatA treated cells demonstrated shortened survival, indicating decreased persistence following degranulation, with a median time of 13.7 minutes for 50% survival compared to 28.8 minutes for control treated cells. This suggests that the shortened survival of those that degranulated was a feature of their being withdrawn, thus implying a role for actin in maintaining the degranulated granule at the cortex prior to its withdrawal into the cells.

The difference in persistence, however, still did not exclude a more rapid loss of green fluorescence following degranulation in LatA-treated owing to faster dissipation of granule contents and/or the granule membrane. To help discriminate between the two models (dissipation and withdrawal), the area and mean fluorescent intensity (MFI) of granules in LatA- or DMSO-treated cells was measured at 10-second intervals following degranulation (pHluorin fluorescence). Specifically, were there to be increased dissipation in the absence of actin integrity there should be increased area of pHluorin signal observed immediately after degranulation in the LatA-treated cells. There was a significantly greater sum fluorescent intensity (MFI*area) of granules from DMSO treated cells up to forty minutes post-degranulation at almost all time points tested (figure 8B, $p<0.0001$ by Mann Whitney U test). This was in spite of a slightly greater area of granules from LatA treated cells, as seen in Figure 8C. This difference in area was significant by Mann Whitney U test over 40 minutes ($p<0.0001$). This difference, however, may have been partially due to fewer granules remaining, thereby weighting the results in favor of the few remaining larger granules. Truncation of the measurements at an earlier time (20 minutes post degranulation) resulted in loss of significance in granule area, suggesting the difference may not be physiologically relevant ($p=0.4$, Supplementary Figure 1A). Interestingly, truncation at 20 minutes did not affect significance of the difference in sum fluorescent intensity ($p<0.0001$, Supplementary Figure 1B). This suggests that over all time points measured, granules from control treated cells had a greater sum fluorescent intensity, likely attributable to an increase in mean fluorescent intensity. Since the intensity over a unit area is a predicted feature of the number of pHluorin molecules from the granule membrane present in the zone of TIRF illumination, and there was not a rapid decline, the result argues against a dissipation model. Instead, it supports a withdrawal model and further suggests that the depolymerization of actin by LatA is preventing the compression of the lytic granule into the NK cell membrane. As a result, the increase in pHluorin signal identified in DMSO-treated control was absent in LatA treated cells. Thus, the role of actin in degranulation after the granule is delivered is predicted to be one of fully extruding granule contents.

DISCUSSION

In this study we have carefully determined the nature of lytic granule kinetics and degranulation in NK cells using pH sensors in combination with TIRFm. We have shown that NK cell lytic granules undergo undirected yet highly dynamic motility prior to, but not immediately preceding or following, degranulation. Importantly, once granules are delivered to the IS, actin integrity is not required for granule motility at the cell cortex immediately preceding degranulation, but instead for the persistence of granules following it.

A longstanding paradigm applied to granule secretion in both NK cells and CTLs has been that granules are secreted through a central clearance, devoid of actin, to which granules are delivered directly by the MTOC (6, 18). However, recently in NK cells this has been challenged by the observation that a filamentous actin meshwork is present throughout the activating synapse, and that granules are secreted through minimally permissive actin

NIH-PA Author Manuscript

NIH-PA Author Manuscript

NIH-PA Author Manuscript

hypodensities (5, 19). While NK cell granules can be secreted centrally (19), in NK92 and ex vivo human NK cells granules have also been observed being exocytosed throughout the synapse ((5), unpublished observations). In CTL, while granules are delivered to the plasma membrane in a central area, they are also observed to travel at the cell cortex from the periphery under conditions of low affinity peptide-MHC interaction (20). Taken together, these results suggest that granules are not simply centrally ejected directly from the MTOC, but may also undergo movement at the plasma membrane prior to exocytosis. Our initial observation of a delay between granule polarization, degranulation and target cell death (Figures 1 & 2), led us to investigate the dynamics of granules at the plasma membrane, revealing highly dynamic, apparently undirected movement of granules prior to exocytosis. In addition, high resolution TIRFm showed that granules polarizing to the cell membrane have variable fates. These include persistence, degranulation and withdrawal from the cortex following variable periods of motility at the plasma membrane.

The mechanism responsible for lytic granule movement after they have been delivered to the synapse in NK cells is unknown. We investigated whether actin remodeling, and integrity at this relatively late time point after synapse formation was a requirement for granule motility. In resting human NK cells, treatment with Latrunculin B arrests those granules constitutively found at the plasma membrane, suggesting actin dependent movement (21). Myosin IIA is enriched on lytic granules and enables the interaction of granules with actin, and inhibition of myosin light kinase reduces the penetration into the cortex as well as the motility of granules existing within the cortex, again suggesting actin-dependent movement of cortical granules (9). However, surprisingly, here we found that LatA treatment (which completely depolymerizes cortical actin (5)) did not significantly affect granule movement prior to degranulation, as the velocity and displacement of granules was comparable between control- and LatA-treated cells. Granule movement at the cortex may be mediated by microtubules. Granules move on microtubules in a dynein-dependent manner prior to MTOC polarization (4). In CTL, granules move in a plus-ended, kinesin-mediated direction and kinesin-1 is required to enable delivery of granules from the MTOC to the plasma membrane following MTOC polarization (22, 23). In addition, treatment of resting human NK cells with nocodazole arrests the movement of granules at the cortex (21). Our results in activated NK cells, taken together with those previously reported in otherwise resting NK cells (21), suggest that NK cells may employ multiple mechanisms of granule movement, including activation-specific, actin-independent movement. Interestingly, in neutrophils, disruption of actin by cytochalasin D treatment does not prevent movement of their granules in the TIRF plane at the membrane, but instead seems to promote the accumulation of these granules at the exocytic zone. This suggests that actin remodeling is not required for lateral movement, but instead may be required for clearing the way for granules through cortical actin (24). This may reflect commonality between cells of the innate immune system and their mechanism of secretion. With that being said, Latrunculin B treatment does not result in increased numbers of granules at the plasma membrane in resting human NK cells (21), and we did not observe any gross accumulation of granules at the activated NK IS in the presence of Latrunculin A (data not shown).

While not required for granule movement prior to exocytosis, however, we demonstrate that actin dynamics affect the post-degranulation process. Specifically, actin is required for the persistence of granules at the membrane following degranulation. This is consistent with a role for F-actin in the expulsion of granule contents, the tethering of granules at the cortex, or the retention of granule contents at the plasma membrane to prevent diffusion. Our data are consistent with the first two of these models (Figure 9A). While there was some difference in the area of granules from LatA treated cells at later time points, which could support a role for actin in the prevention of lateral diffusion, this may have been due to the bias of the measurement of a few granules that had survived to this time. At all times,

NIH-PA Author Manuscript

NIH-PA Author Manuscript

NIH-PA Author Manuscript

however, there was a significant difference in fluorescent intensity of granules following degranulation from LatA-treated cells that did not correspond to an increase in area. This suggests that actin is not required to simply act as a fence preventing the diffusion of granule contents, but may serve as a platform for the generation of force resulting in the squeezing of contents from the granule as well as act as a tether to retain the granule at the cortex. This model is consistent with other cell types in which actin has been considered to be both a barrier to, and permissive of, granule exocytosis. In PC12 chromaffin cells, treatment with LatA results in a more rapid expulsion of granule contents, which would be consistent with our observation of shorter persistence of fluorescence post-degranulation (25). Together, these results suggest a requirement for force in fully extracting lytic components from granules, which contain a dense core including extracellular matrix components such as proteoglycans (26, 27). It should also be noted that, while we did not observe a difference in granule velocity or displacement, we did see a significant difference between control and LatA-treated cells in displacement rate, with LatA-treated cells having a significantly lower displacement rate pre-degranulation. This observation also supports a model in which actin may function in the tethering or catching of granules. Finally, actin remodeling may be required for the formation of permissive clearances in the cortex. However, while not quantified here, there was no observable defect in the number of granules that reached the TIRF plane in LatA-treated cells, consistent with prior reports (21).

The observation that granules undergo dynamic motility for such a substantive amount of time is somewhat surprising. The seemingly undirected nature of the movement may reflect a need for the granule to travel to a point of suitable actin clearance in order to be secreted. It may also indicate a requirement for granules to seek docking domains for membrane tethering and fusion. The observation that granules undergo slowing and arrest of movement regardless of whether or not they degranulate (Figure 6F) suggests that a sustained presence at the cell cortex ultimately results in arrest for most granules. As described in the model in Figure 9B, however, there seem to be multiple outcomes for granules that polarize to the synapse. These include degranulation, persistence or withdrawal. It is unclear what the relationship between these models is, particularly as motility does not predict degranulation or lack thereof.

In conclusion, our results demonstrate a previously unreported dynamic motility of NK cell granules prior to, but not following, degranulation. To our knowledge they include the first demonstration of degranulation in a living NK cell in conjugation with its target cell. They also show a surprising role of actin dynamics in post-degranulation, but not pre-degranulation, granule behavior at the activating NK cell synapse. This implies that in addition to serving a role early after synapse formation in enabling NK cell lytic granule localization towards the target cell, the synaptic actin meshwork facilitates the compression of lytic granules. This would define a role for actin in the optimal extrusion of lytic granule contents by serving as a platform for the generation of force by which the granule contents are fully emptied.

Supplementary Material

Refer to Web version on PubMed Central for supplementary material.

Acknowledgments

We thank Dr. G. Rak for technical assistance.

NIH-PA Author Manuscript

NIH-PA Author Manuscript

NIH-PA Author Manuscript

References

1. Orange JS. Formation and function of the lytic NK-cell immunological synapse. Nat Rev Immunol. 2008; 8:713–725. [PubMed: 19172692]
2. Wulfing C, Purtic B, Klem J, Schatzle JD. Stepwise cytoskeletal polarization as a series of checkpoints in innate but not adaptive cytolytic killing. Proc Natl Acad Sci U S A. 2003; 100:7767–7772. [PubMed: 12802007]
3. Zarcone D, Prasthofer EF, Malavasi F, Pistoia V, LoBuglio AF, Grossi CE. Ultrastructural analysis of human natural killer cell activation. Blood. 1987; 69:1725–1736. [PubMed: 3107633]
4. Mentlik AN, Sanborn KB, Holzbaur EL, Orange JS. Rapid lytic granule convergence to the MTOC in natural killer cells is dependent on dynein but not cytolytic commitment. Mol Biol Cell. 2010; 21:2241–2256. [PubMed: 20444980]
5. Rak GD, Mace EM, Banerjee PP, Svitkina T, Orange JS. Natural killer cell lytic granule secretion occurs through a pervasive actin network at the immune synapse. PLoS Biol. 2011; 9:e1001151. [PubMed: 21931536]
6. Orange JS, Harris KE, Andzelm MM, Valter MM, Geha RS, Strominger JL. The mature activating natural killer cell immunologic synapse is formed in distinct stages. Proc Natl Acad Sci U S A. 2003; 100:14151–14156. [PubMed: 14612578]
7. Brown AC, Oddos S, Dobbie IM, Alakoskela JM, Parton RM, Eissmann P, Neil MA, Dunsby C, French PM, Davis I, Davis DM. Remodelling of cortical actin where lytic granules dock at natural killer cell immune synapses revealed by super-resolution microscopy. PLoS Biol. 2011; 9:e1001152. [PubMed: 21931537]
8. Mace EM, Orange JS. Dual channel STED nanoscopy of lytic granules on actin filaments in natural killer cells. Communicative & Integrative Biology. 2012; 5:1. [PubMed: 22482000]
9. Sanborn KB, Rak GD, Maru SY, Demers K, Difeo A, Martignetti JA, Betts MR, Favier R, Banerjee PP, Orange JS. Myosin IIA associates with NK cell lytic granules to enable their interaction with F-actin and function at the immunological synapse. J Immunol. 2009; 182:6969–6984. [PubMed: 19454694]
10. Andzelm MM, Chen X, Krzewski K, Orange JS, Strominger JL. Myosin IIA is required for cytolytic granule exocytosis in human NK cells. J Exp Med. 2007; 204:2285–2291. [PubMed: 17875677]
11. Orange JS, Roy-Ghanta S, Mace EM, Maru S, Rak GD, Sanborn KB, Fasth A, Saltzman R, Paisley A, Monaco-Shawver L, Banerjee PP, Pandey R. IL-2 induces a WAVE2-dependent pathway for actin reorganization that enables WASp-independent human NK cell function. J Clin Invest. 2011; 121:1535–1548. [PubMed: 21383498]
12. Banerjee PP, Pandey R, Zheng R, Suhoski MM, Monaco-Shawver L, Orange JS. Cdc42-interacting protein-4 functionally links actin and microtubule networks at the cytolytic NK cell immunological synapse. J Exp Med. 2007; 204:2305–2320. [PubMed: 17785506]
13. Peters PJ, Borst J, Oorschot V, Fukuda M, Krahenbuhl O, Tschopp J, Slot JW, Geuze HJ. Cytotoxic T lymphocyte granules are secretory lysosomes, containing both perforin and granzymes. J Exp Med. 1991; 173:1099–1109. [PubMed: 2022921]
14. Alter G, Malenfant JM, Altfeld M. CD107a as a functional marker for the identification of natural killer cell activity. J Immunol Methods. 2004; 294:15–22. [PubMed: 15604012]
15. Miesenbock G, De Angelis DA, Rothman JE. Visualizing secretion and synaptic transmission with pH-sensitive green fluorescent proteins. Nature. 1998; 394:192–195. [PubMed: 9671304]
16. Bryceson YT, March ME, Barber DF, Ljunggren HG, Long EO. Cytolytic granule polarization and degranulation controlled by different receptors in resting NK cells. J Exp Med. 2005; 202:1001–1012. [PubMed: 16203869]
17. Butler B, Cooper JA. Distinct roles for the actin nucleators Arp2/3 and hDia1 during NK-mediated cytotoxicity. Curr Biol. 2009; 19:1886–1896. [PubMed: 19913427]
18. Stinchcombe JC, Majorovits E, Bossi G, Fuller S, Griffiths GM. Centrosome polarization delivers secretory granules to the immunological synapse. Nature. 2006; 443:462–465. [PubMed: 17006514]

NIH-PA Author Manuscript

NIH-PA Author Manuscript

NIH-PA Author Manuscript

19. Brown AC, Oddos S, Dobbie IM, Alakoskela JM, Parton RM, Eissmann P, Neil MA, Dunsby C, French PM, Davis I, Davis DM. Remodelling of cortical actin where lytic granules dock at natural killer cell immune synapses revealed by super-resolution microscopy. PLoS Biol. 2011; 9:e1001152. [PubMed: 21931537]

20. Beal AM, Anikeeva N, Varma R, Cameron TO, Vasiliver-Shamis G, Norris PJ, Dustin ML, Sykulev Y. Kinetics of early T cell receptor signaling regulate the pathway of lytic granule delivery to the secretory domain. Immunity. 2009; 31:632–642. [PubMed: 19833088]

21. Liu D, Meckel T, Long EO. Distinct role of rab27a in granule movement at the plasma membrane and in the cytosol of NK cells. PLoS One. 2010; 5:e12870. [PubMed: 20877725]

22. Burkhardt JK, McIlvain JM Jr, Sheetz MP, Argon Y. Lytic granules from cytotoxic T cells exhibit kinesin-dependent motility on microtubules in vitro. J Cell Sci. 1993; 104(Pt 1):151–162. [PubMed: 8449993]

23. Kurowska M, Goudin N, Nehme NT, Court M, Garin J, Fischer A, de Saint Basile G, Menasche G. Terminal transport of lytic granules to the immune synapse is mediated by the kinesin-1/Slp3/Rab27a complex. Blood. 2012; 119:3879–3889. [PubMed: 22308290]

24. Johnson JL, Monfregola J, Napolitano G, Kiosses WB, Catz SD. Vesicular trafficking through cortical actin during exocytosis is regulated by the Rab27a effector JFC1/Slp1 and the RhoA-GAP GMIP. Mol Biol Cell. 2012

25. Wang J, Richards DA. Spatial regulation of exocytic site and vesicle mobilization by the actin cytoskeleton. PLoS One. 2011; 6:e29162. [PubMed: 22195014]

26. Burkhardt JK, Hester S, Argon Y. Two proteins targeted to the same lytic granule compartment undergo very different posttranslational processing. Proc Natl Acad Sci U S A. 1989; 86:7128–7132. [PubMed: 2674947]

27. MacDermott RP, Schmidt RE, Caulfield JP, Hein A, Bartley GT, Ritz J, Schlossman SF, Austen KF, Stevens RL. Proteoglycans in cell-mediated cytotoxicity. Identification, localization, and exocytosis of a chondroitin sulfate proteoglycan from human cloned natural killer cells during target cell lysis. J Exp Med. 1985; 162:1771–1787. [PubMed: 3934316]

NIH-PA Author Manuscript
NIH-PA Author Manuscript
NIH-PA Author Manuscript

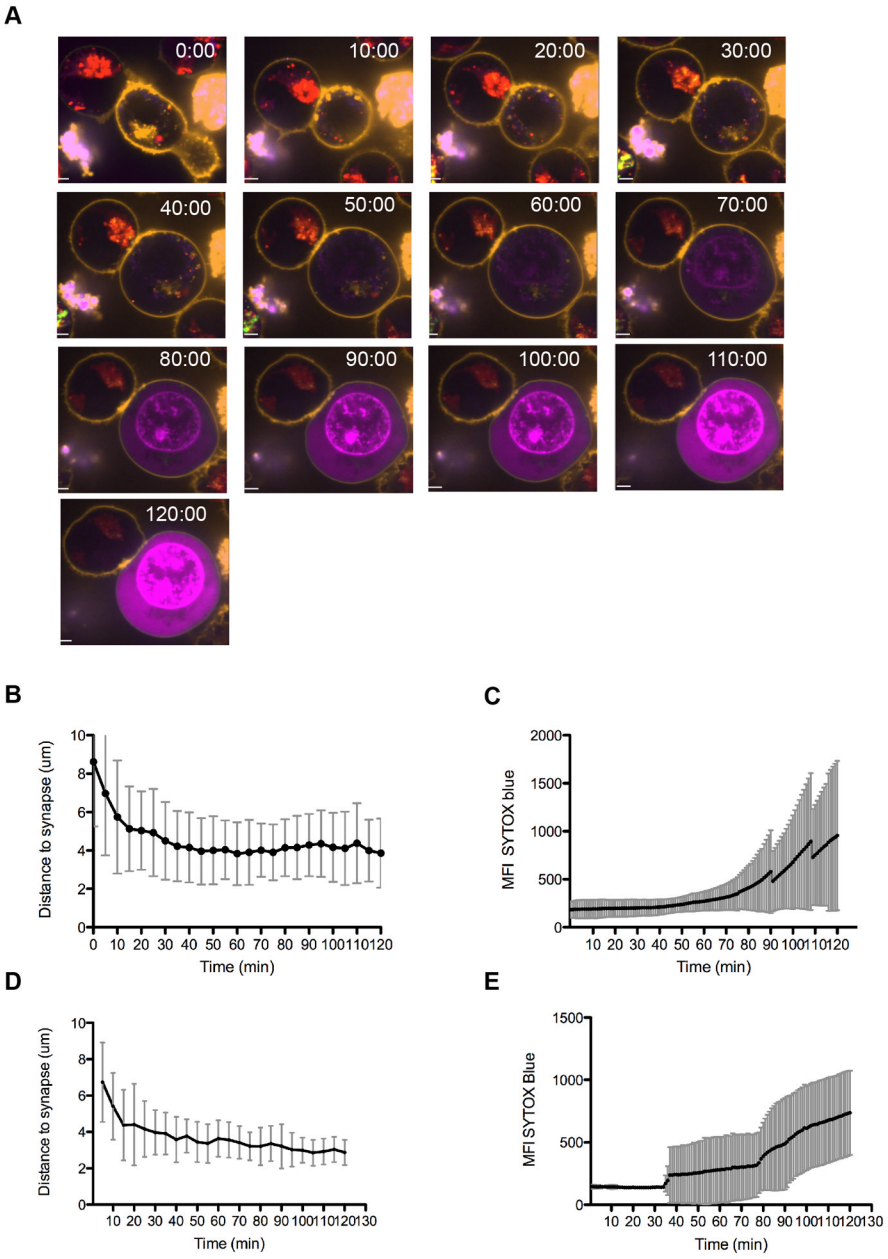

Figure 1. Lytic granule polarization precedes persistence at the NK immunological synapse prior to target cell death

YTS GFP-actin (A, B, C) or NK92 GFP-tubulin (D, E) NK cells were loaded with LysoTracker Red (red) and incubated with CellMask labeled 721.221 (A, B, C) or K562 (D, E) target cells in the presence of SYTOX Blue (blue) to detect cell death. Conjugates were imaged by confocal microscopy at 1 frame per minute for 90–130 minutes. **A.** Representative YTS GFP-actin-721.221 conjugate is shown at 10-minute intervals for 120 minutes. Scale bar=1 um. **B.** Time to granule polarization in YTS GFP-actin NK cells as measured by lytic granule centroid distance to IS (mean 41.5±12 minutes, n=10). **C.** Time to initiation of 721.221 target cell apoptosis as detected by SYTOX Blue entry is shown for 10 conjugates (mean 61.5 ± 10 minutes, n=10). **D.** Time to granule polarization in NK92 GFP-tubulin NK cells as measured by lytic granule centroid distance to IS (mean 24.2 minutes,

NIH-PA Author Manuscript

NIH-PA Author Manuscript

NIH-PA Author Manuscript

n=6). **E.** Time to initiation of K562 target cell apoptosis as detected by SYTOX Blue entry is shown for 10 conjugates (mean 54.2 minutes, n=6). All representative images and analyses shown are from 4 independent experiments. Error bars indicate SD.

NIH-PA Author Manuscript
NIH-PA Author Manuscript
NIH-PA Author Manuscript

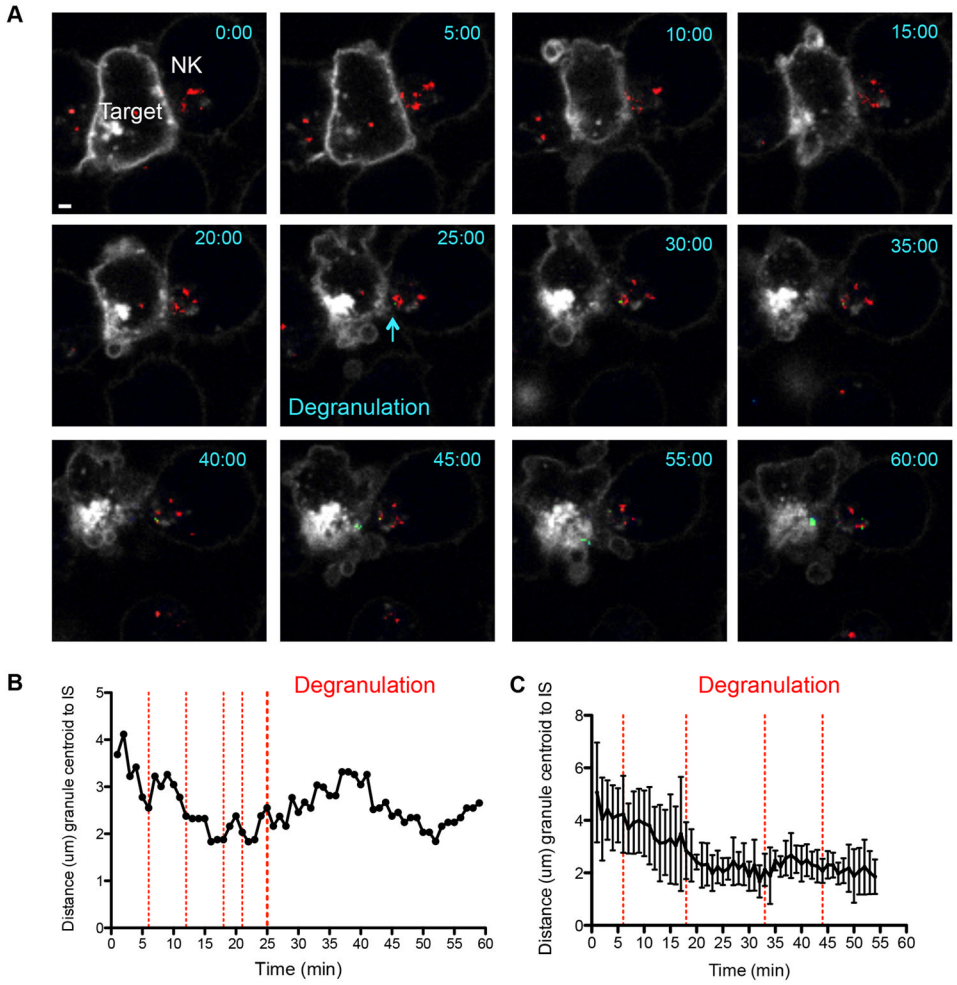

Figure 2.

Visualization of NK cell lytic granule polarization and degranulation by live cell confocal microscopy. NK92 cells expressing pHlourin-LAMP1 (green) were loaded with LysoTracker Red (red) and incubated with Cell Mask labeled K562 cells as in Figure 1. Conjugates were imaged by confocal microscopy at 1 frame per minute for 90–130 minutes. **A.** One representative conjugate from 4 independent experiments is shown at 10-minute intervals for 60 minutes. One degranulation event is shown at 25 minutes. Scale bar = 1 μm. **B.** Granule polarization in representative NK92 pHlourin-LAMP1 cell shown in A as measured in Figure 1. Red vertical dashed lines indicate brief individual degranulation events prior to the sustained event beginning at 25 minutes (heavy red dashed line). **C.** Mean granule polarization from 4 independent experiments (n = 4) with vertical red lines indicating initial degranulation events from each conjugate analyzed. Error bars indicate SD.

NIH-PA Author Manuscript

NIH-PA Author Manuscript

NIH-PA Author Manuscript

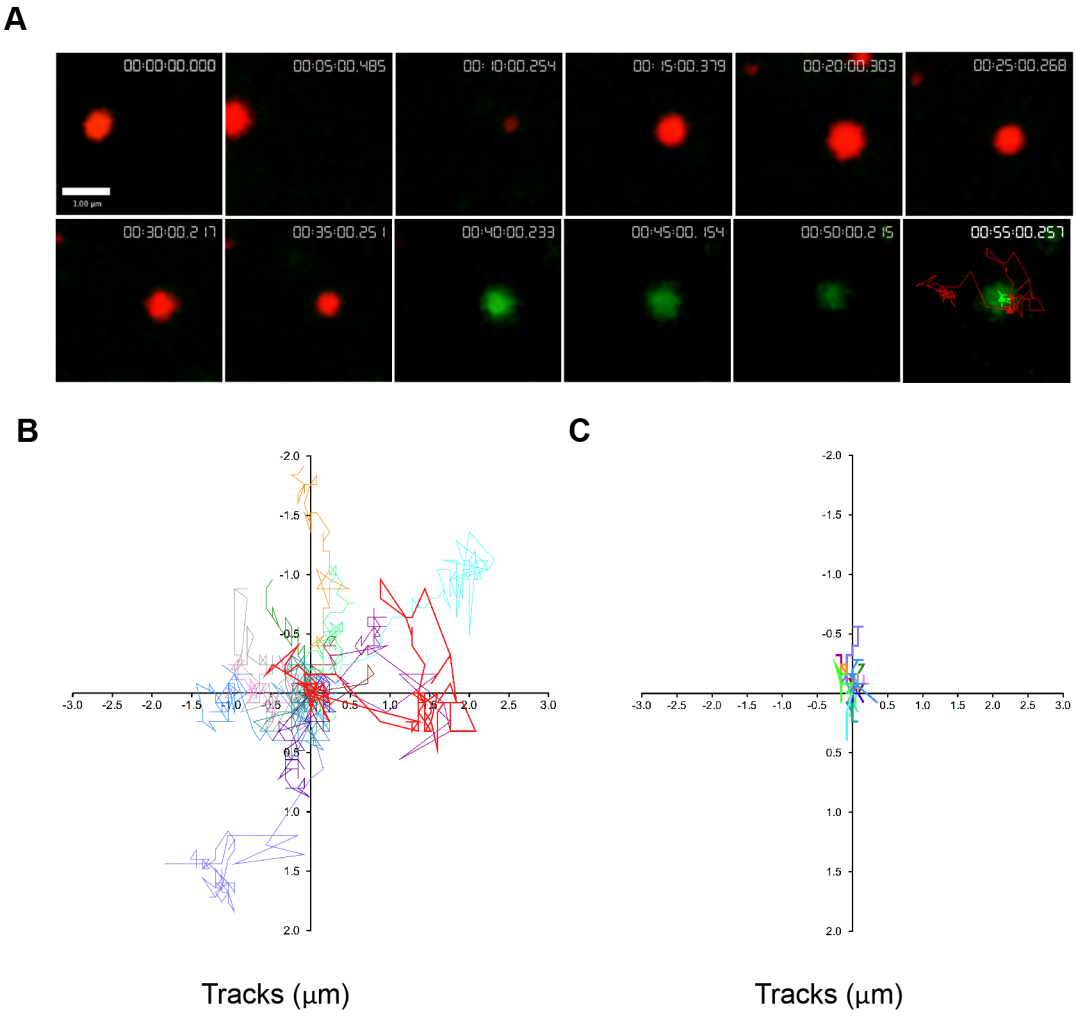

Figure 3. Lytic granules navigate the cell cortex prior to degranulation

NK92 cells expressing pHlourin-LAMP1 (green) were loaded with LysoTracker Red (red) and activated by immobilized antibody to NKp30 and CD18. Cells were imaged by TIRFm at 6 frames per minute for 60–80 minutes. **A.** Representative NK92 lytic granule is shown at 5-minute intervals following 10 minutes of cell contact with the activating surface. Granules were tracked using Volocity software prior to and following degranulation as described in *Materials and Methods*. Pre-degranulation LysoTracker Red (red) and post-degranulation pHluorin-LAMP1 (green) tracks are shown in the final 55-minute image. Scale bar=1 μm. **B.** Overlay of LysoTracker Red tracks of 14 pre-degranulation events over 4 separate experiments. Lytic granule track from (A) shown in bold (red). **C.** Overlay of pHluorin-LAMP1 tracks of corresponding degranulation events. Lytic granule track from (A) shown in bold (green).

NIH-PA Author Manuscript

NIH-PA Author Manuscript

NIH-PA Author Manuscript

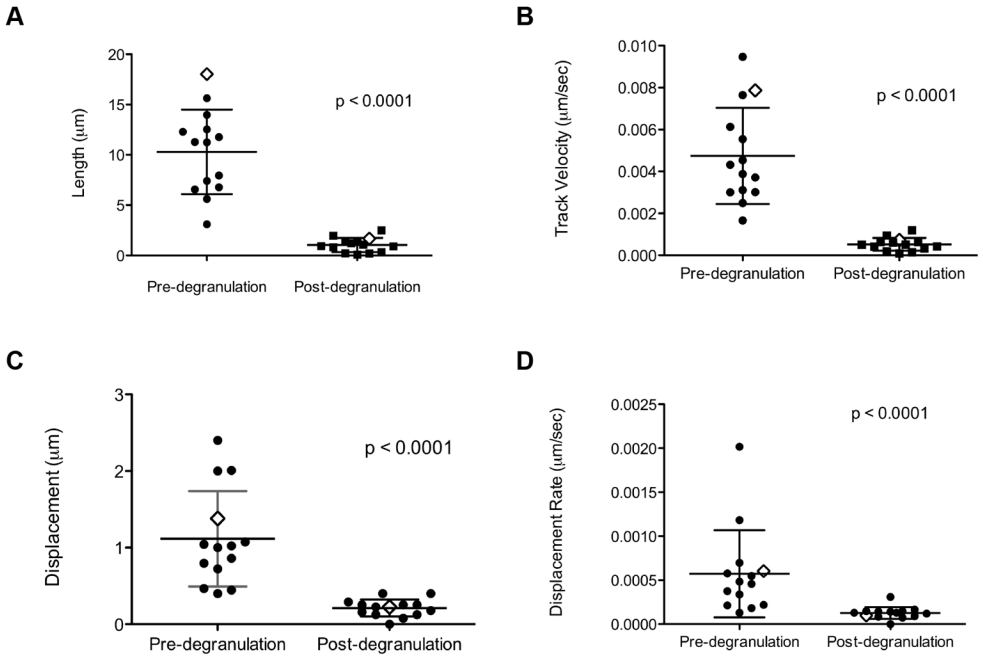

Figure 4. Synaptic lytic granules show greater motility prior to degranulation

Granule tracks were analyzed using Volocity software as described in Materials and Methods. Granule track length **(A)**, track velocity **(B)**, displacement **(C)**, and displacement rate **(D)** from 14 events pre- (LysoTracker Red, left) and post-degranulation (pHlourin-LAMP1, right) are shown. Representative NK92 lytic granules from Figure 3A are indicated by open diamonds. Mean ± SD are shown. Differences between Lysotracker Red and pHlourin-LAMP1 granule tracks were significant ($p < 0.0001$, two-tailed *t* test). Results are from 4 independent experiments.

NIH-PA Author Manuscript
NIH-PA Author Manuscript
NIH-PA Author Manuscript

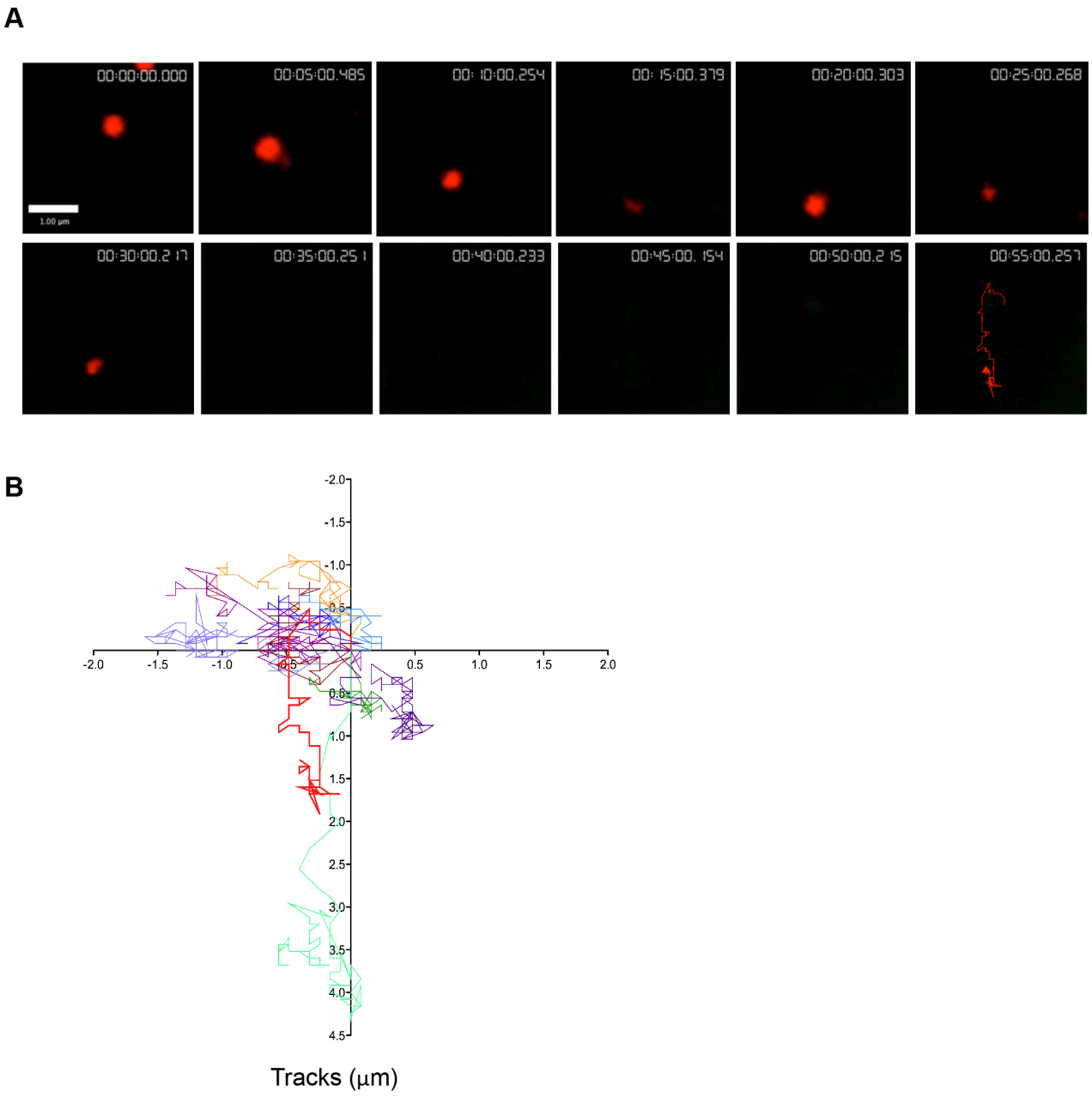

Figure 5. Lytic granules that do not degranulate show normal synaptic motility

Lytic granules demonstrating no observed degranulation were analyzed. **A.** Representative NK92 lytic granule cropped from image sequence is shown at 5-minute intervals following 10 minutes of contact. Lysotracker Red (red) track denoting all observed timepoints is shown in final 55-minute image. Scale bar=1 μm. **B.** Overlay of LysoTracker Red tracks of 10 lytic granules over 4 separate experiments. Representative granule track from (A) is depicted in bold (red).

NIH-PA Author Manuscript

NIH-PA Author Manuscript

NIH-PA Author Manuscript

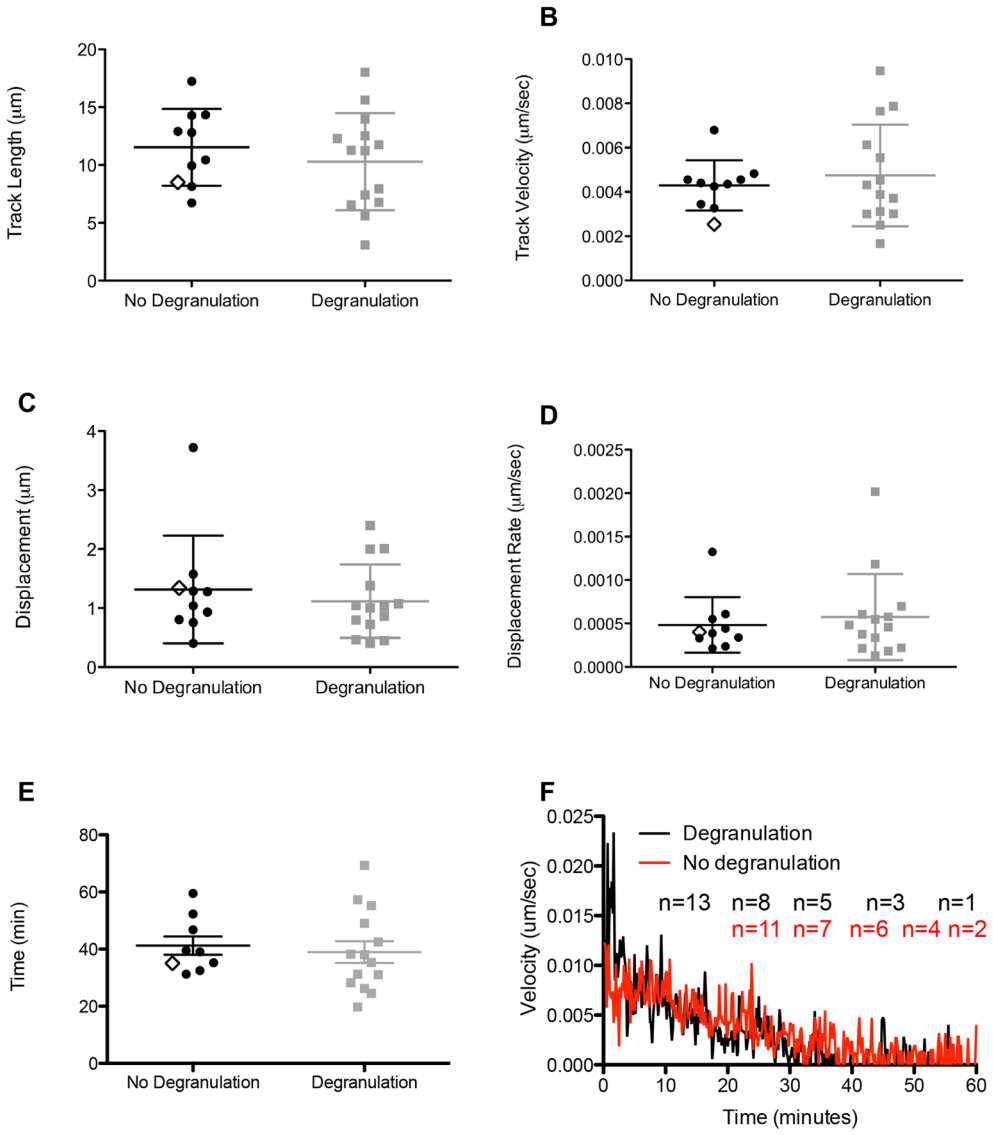

Figure 6. Characteristics of synaptic lytic granule motility that do not degranulate

Comparative measurements of LysoTracker Red motility in lytic granules for which degranulation or no degranulation was observed. Length **(A)**, track velocity **(B)**, displacement **(C)**, displacement rate **(D)**, and persistence time **(E)** plotted for 10 granules observing no degranulation (LysoTracker Red only). Data is shown alongside measurements obtained from degranulation events previously illustrated in Figure 4 (i.e., the same results in Figure 3 for degranulating granules). The representative NK92 granule from Figure 5A is indicated in LysoTracker Red data set for comparison to the other granules measured, but for which image sequences are not shown (open diamond). F) Velocities of granules that degranulate (black) or do not (red) were measured at one minute intervals. Mean ± SD are depicted. The means of the LysoTracker Red data sets were not significantly different ($p>0.05$, two-tailed *t* test). Results are shown from 4 independent experiments.

NIH-PA Author Manuscript
NIH-PA Author Manuscript
NIH-PA Author Manuscript

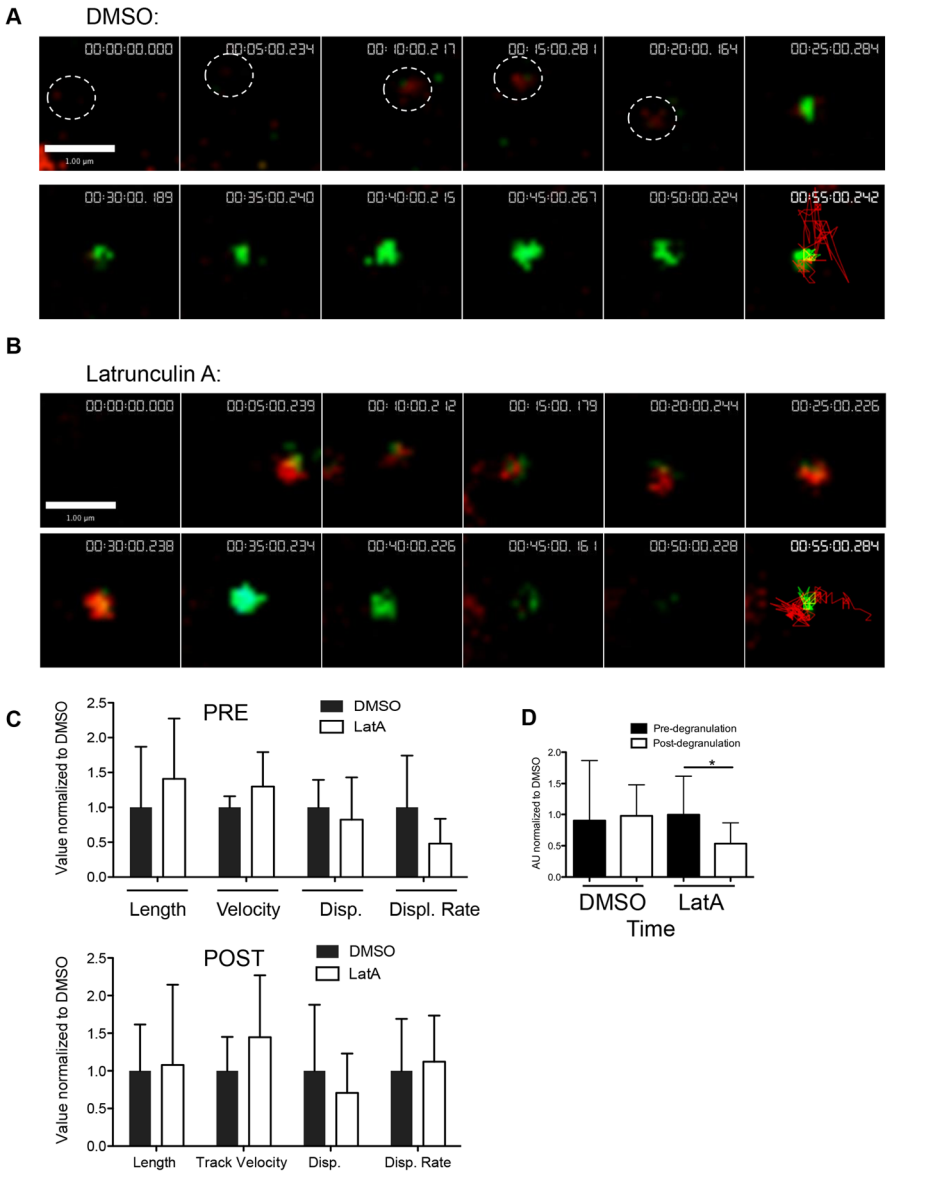

Figure 7. Effect of actin depolymerization upon synaptic lytic granule kinetics

NK92 cells expressing pHlourin-LAMP1 (green) were loaded with LysoTracker Red (red) and activated upon immobilized antibody to NKp30 and CD18. Cells were imaged by TIRF microscopy at 6 frames per minute for 60–80 minutes. A representative NK92 lytic granule cropped from the image sequence is shown at 5-minute intervals following 5–10 minutes of contact-induced activation. LysoTracker Red and pHluorin-LAMP1 tracks depicting the course of the granule over all timepoints are shown in final 55-minute image. Scale bars=1 μm. **A.** Vehicle control (DMSO) was added 10–20 minutes following the addition of cells to the imaging chamber. The white circle indicates granules location in frames 1–5. **B**. LatA was added between 10 and 15 minutes for a final concentration of 10 μM. **C.** Measured mean characteristics of synaptic lytic granule motility before (black bars) and after (white bars) degranulation. Mean track length, track velocity, displacement, displacement rate, and timespan of lytic granules are all shown relative to the respective DMSO values, which have been normalized to 1. Mean ± SD are shown. Significant differences between DMSO- and

Latrunculin A-treated granule tracks are marked with an asterisk ($p<0.05$, two-tailed t test). Results shown are from 4 independent experiments.

NIH-PA Author Manuscript
NIH-PA Author Manuscript
NIH-PA Author Manuscript

NIH-PA Author Manuscript
NIH-PA Author Manuscript
NIH-PA Author Manuscript

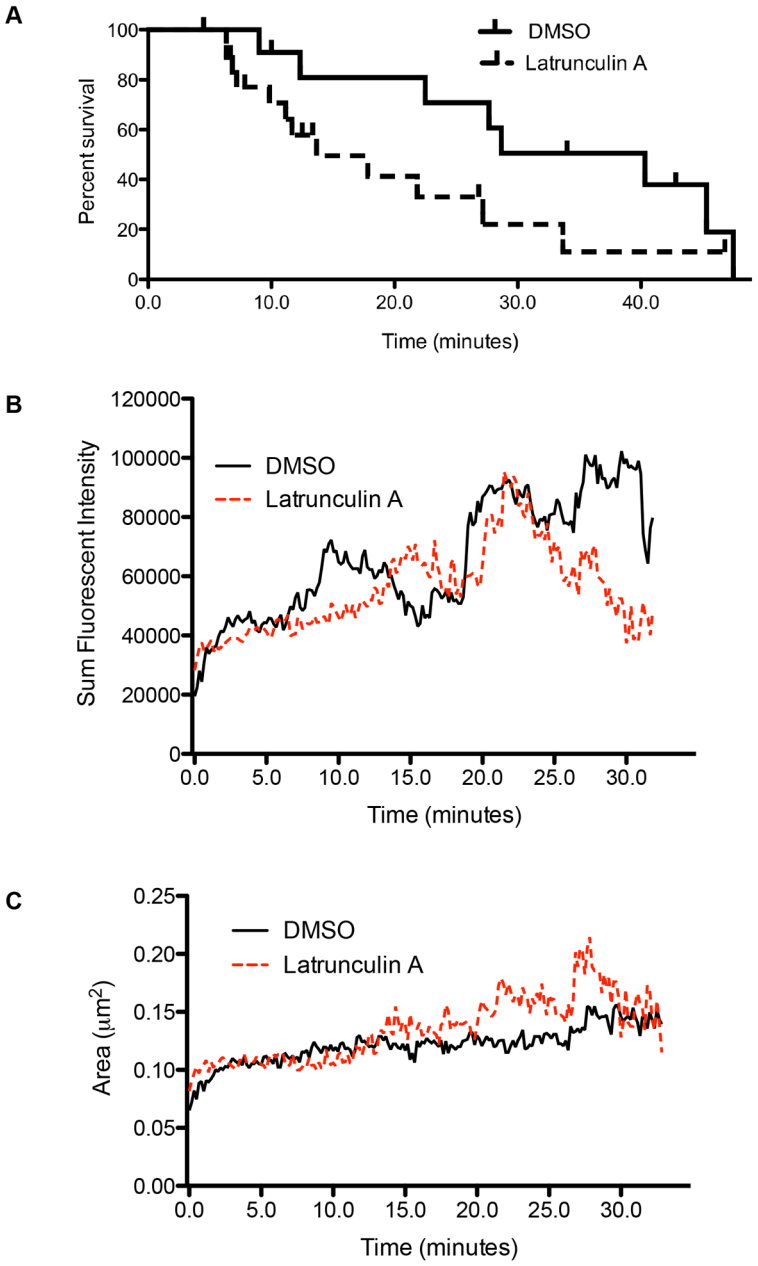

Figure 8. The synaptic actin network is required for the persistence of degranulation

A. The lifetime of lytic granules post-degranulation in NK cells treated with LatA or DMSO control. Time points reflect amount of time elapsed post-degranulation (marked by the appearance of LAMP1-phluorin) with vertical drops indicating disappearance of the granule from TIRF field. Vertical ticks indicate granules persisting to the end of the imaging sequence. **B.** Area of the observed lytic granules in cells treated with DMSO (solid black), or LatA (dashed red). **C.** Sum fluorescent intensity of lytic granules in NK92 cells expressing pHluorin-LAMP1. Cells were treated with DMSO (solid black), or LatA (dashed red) as per Figure 7. Note that sum fluorescent intensity is a function of both the area and mean fluorescent intensity of a lytic granule. Granule boundaries were defined using fluorescent intensity with 3 SD above background as a cutoff. Results shown are from 4 independent experiments.

NIH-PA Author Manuscript

NIH-PA Author Manuscript

NIH-PA Author Manuscript

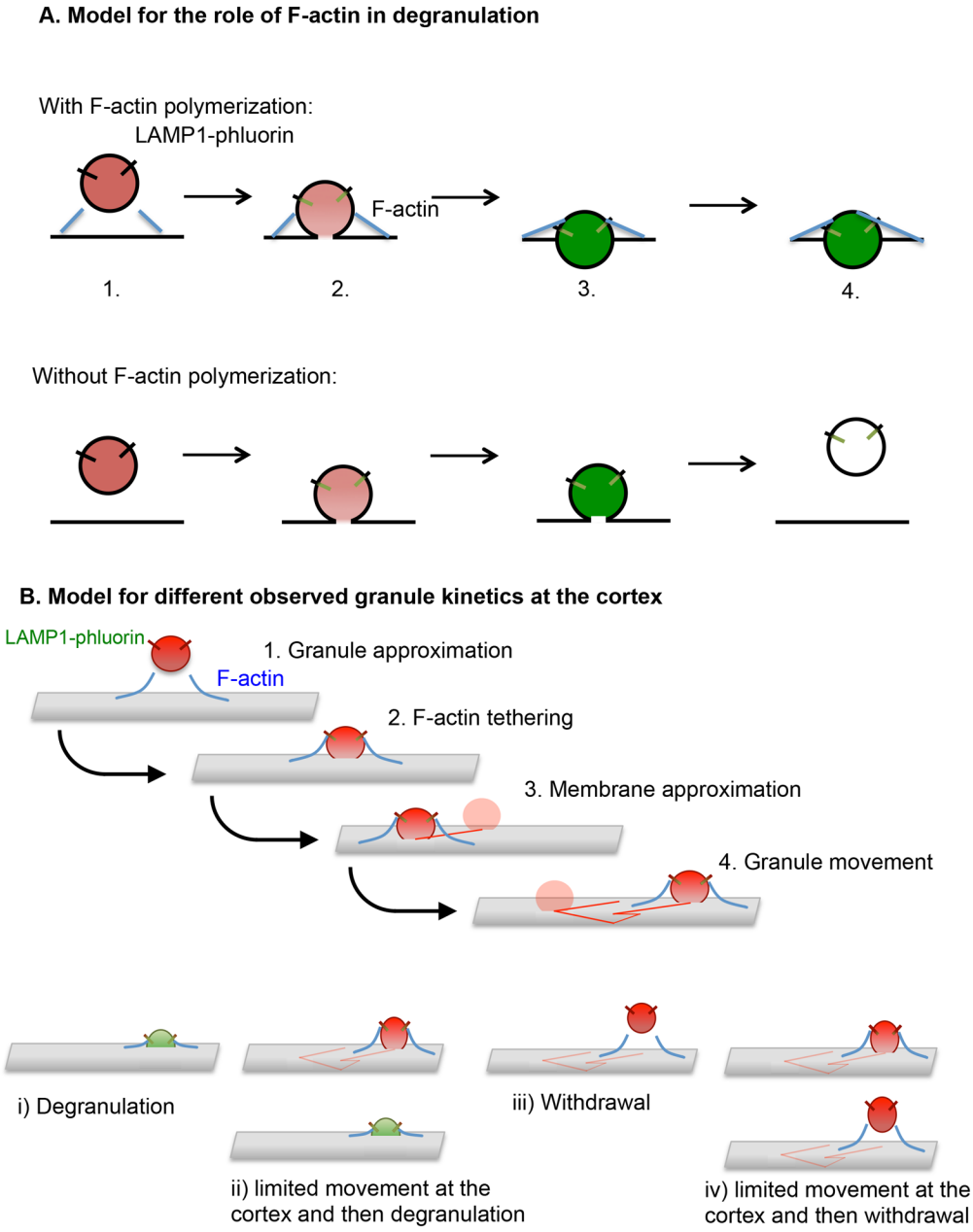

Figure 9. Models for the role of F-actin in granule persistence and the varying behavior of lytic granules at the NK cell cortex

A) A LysoTracker Red-loaded LAMP1-pHlourin expressing granule is depicted approaching within cell cortex nearing a region within the F-actin network suitable for membrane access (as previously demonstrated (5, 7) **(1)**. As docking and fusion occurs **(2)**, F-actin acts as a tether to help anchor the granule at the membrane, although in both cases fusion results in the activation of LAMP1-phluorin and the subsequent appearance of green fluorescence. In addition, actin reorganization is likely to act in the generation of force to aid in the focused expulsion of granule contents (as supported by greater area*intensity of pHluorin-LAMP1 in control-compared to LatA-treated cells) **(3)** and the continued persistence of the degranulating granule at the cortex which we would propose is a feature of the interaction of the granule with the local F-actin network **(4)**. B) A LysoTracker Red

loaded LAMP1-pHlourin expressing granule approaches the cell membrane and docks with the aid of F-actin tethering (1, 2). This is followed by the approximation of the granule to the cell cortex, movement, then one of the outcomes depicted below. i) immediate exocytosis, ii) limited movement and exocytosis, iii) immediate withdrawal from the cortex or iv) limited movement before withdrawal.

NIH-PA Author Manuscript
NIH-PA Author Manuscript
NIH-PA Author Manuscript